

Università degli Studi di Napoli “Federico II”



**SCUOLA POLITECNICA E DELLE SCIENZE DI BASE
DIPARTIMENTO DI INGEGNERIA INDUSTRIALE**

**CORSO DI LAUREA IN INGEGNERIA AEROSPAZIALE
CLASSE DELLE LAUREE IN INGEGNERIA INDUSTRIALE (L-9)**

Elaborato di laurea in Meccanica del Volo
**Geometric modelling, stability and control analysis
of the F-35 fighter aircraft with OpenVSP**

**Relatore:
Prof. Danilo Ciliberti**

**Candidato:
Roberta Di Maio
Matr. N35004107**

ANNO ACCADEMICO 2024 – 2025

Ai miei genitori

Abstract

This work aims to analyze the fifth-generation multirole aircraft F-35 Lightning II, focusing on its geometric modeling, stability and control characteristics. After a historical introduction outlining the background that led to the development of the Joint Strike Fighter program, the three variants of the F-35 are examined, comparing their structural configurations, propulsion architectures, and specific operational roles. In the following chapters, a three-dimensional model of the F-35 Lightning II is presented, developed using the OpenVSP software. Using the integrated tools, a preliminary assessment of the aircraft's stability and control characteristics was carried out, with specific reference to the VSPAERO module. Although the software presents some inherent limitations—both in terms of geometric representation and analytical precision—it nonetheless proves to be a useful and effective tool for early-stage evaluations of simplified aerodynamic configurations. The results obtained can later be compared with experimental data from wind tunnel tests or with more advanced simulations performed using high-fidelity numerical codes. This work thus aims to offer an engineering and systemic perspective on one of the most ambitious projects in modern military aviation.

Sommario

Il presente lavoro si propone di analizzare il velivolo multiruolo di quinta generazione F-35 Lightning II in termini di modellazione geometrica, caratteristiche di stabilità e controllo. Dopo un'introduzione storica sul contesto che ha portato allo sviluppo del programma Joint Strike Fighter, si analizzano le tre varianti dell'F-35, confrontandone le configurazioni strutturali, le architetture propulsive e le diverse capacità di impiego. Nei capitoli successivi viene illustrato un modello tridimensionale del velivolo F-35 Lightning II, sviluppato tramite l'utilizzo del software OpenVSP. Avvalendosi dei tool integrati, è stata effettuata una valutazione preliminare delle caratteristiche di stabilità e controllo del velivolo, con specifico riferimento al modulo VSPAERO. Nonostante alcune limitazioni intrinseche del software, sia in termini di rappresentazione geometrica che di accuratezza dell'analisi, esso si conferma uno strumento utile ed efficace per indagini preliminari su configurazioni aerodinamiche semplificate. I risultati ottenuti possono essere successivamente confrontati con dati sperimentali da prove in galleria del vento oppure con simulazioni più complesse condotte mediante codici numerici ad alta fedeltà. Il lavoro intende quindi offrire una visione ingegneristica e sistemica di uno dei progetti più ambiziosi della moderna aviazione militare.

Table of contents

1.	F-35 Lightning II.....	6
1.1	Introduction to the F-35 Lightning II Aircraft.....	6
1.2	Program History and Global Collaboration.....	7
1.3	Capabilities and Evolution of the F-35 Lightning II.....	8
1.3.1	Operational Roles and Performance Profile.....	8
1.3.2	Upgrades and Future Development.....	9
1.4	F-35 Variants and Configurational Overview.....	9
2.	OpenVSP.....	11
2.1	VSPAERO.....	11
2.1.1	Core Features and Vortex Theory Foundation.....	12
2.1.2	Surface Tangency Condition and Linear System.....	13
2.1.3	Iterative Solver and Preconditioning.....	14
2.1.4	Computational Complexity and Fast Multipole Strategy.....	14
2.1.5	Wake Modeling and Streamline Adaptation.....	14
3.	Geometric modelling of the F-35A Lightning II.....	16
3.1	Fuselage.....	16
3.2	Wing.....	18
3.3	Horizontal stabilizer.....	20
3.4	Vertical stabilizer.....	21
4.	Longitudinal Aerodynamics Analysis.....	23
4.1	Lift coefficient curves.....	23
4.1.1	Clean configuration.....	23
4.1.2	Effect of Control Surface Deflections on Lift Characteristics.....	24
4.2	Pitching moment coefficient curves.....	26
4.2.1	Clean configuration.....	26

4.2.2	Effect of control surfaces on longitudinal stability	28
4.3	Aerodynamic Polar Analysis of the Aircraft	29
5.	Lateral and Directional Aerodynamics Analysis	32
5.1	Sideforce coefficient C_Y	33
5.2	Yawing moment coefficient CM_z	36
5.3	Rolling moment coefficient CM_x	38
6.	Conclusions	43

List of figures

Figure 1.1	Cutway schematic.....	6
Figure 2.1	Vortex segment	13
Figure 2.2	Curved Wake Lines from VSPAERO.....	15
Figure 3.1	an F-35A model in Open VSP.....	16
Figure 3.2	Alignment of the modeled fuselage with the orthogonal three-view of the F-35A in OpenVSP.....	17
Figure 3.3	OpenVSP “Edit Curve” panel applied to the fuselage cross-section.....	18
Figure 3.4	Cross-sectional view of the NACA 64A210 airfoil.....	19
Figure 3.5	Control surfaces.....	20
Figure 3.6	Configuration of the horizontal stabilator hinge in OpenVSP, showing rotation parameters and attachment to the fuselage.....	21
Figure 3.7	Complete aircraft: mesh visualization	22
Figure 4.1	Lift curve C_L vs α for the clean wing + tail configuration.....	24
Figure 4.2	Effect of wing flap deflection on lift coefficient.....	25

Figure 4.3 Variation of pitching moment coefficient (C_{My}) with angle of attack (α) for two different CG positions.....	27
Figure 4.4 Pitching moment coefficient vs. angle of attack for different flap deflections.....	28
Figure 4.5 Polar curve of the aircraft in clean configuration.....	30
Figure 4.6 Drag polar for clean and deflected flap configurations.....	31
Figure 5.1 Body Reference Frame and Constructive Reference Frame.....	33
Figure 5.2 Flap Deflection Gain.....	33
Figure 5.3 C_Y vs. β with variations of $\delta f = 0^\circ, 15^\circ, 25^\circ$	34
Figure 5.4 Side force coefficient C_Y vs. β for different rudder deflections δr	35
Figure 5.5 Variation of yaw moment coefficient C_{Mz} with sideslip angle β for different rudder deflections δr	36
Figure 5.6 Rolling moment coefficient C_{Mx} vs sideslip angle β for different flap deflections δf	39
Figure 5.7 Spiral trajectory in absence of corrective moments.....	40
Figure 5.8 C_{Mx} vs β for different rudder deflections δr	42

List of tables

Table 1.1 Legacy Aircraft and Corresponding F-35 Variants.....	8
Table 1.2 Comparative Overview of F-35 Variants.....	10

1. F-35 Lightning II

1.1 Introduction to the F-35 Lightning II Aircraft

The F-35 Lightning II, originally developed under the name JSF (Joint Strike Fighter), is an advanced fifth-generation multirole fighter aircraft, single-seat and single-engine, designed to ensure air superiority in operational scenarios with a high density of anti-aircraft defenses. The airframe, composed of approximately 35% composite materials and characterized by a stealth architecture, is optimized to reduce both radar and infrared signatures, also thanks to the implementation of Diverterless Supersonic Inlets (DSI).

The state-of-the-art onboard sensor technology, combined with the aircraft's low observability, enhances its operational effectiveness by ensuring not only increased survivability in hostile environments but also a high level of situational awareness and tactical knowledge.

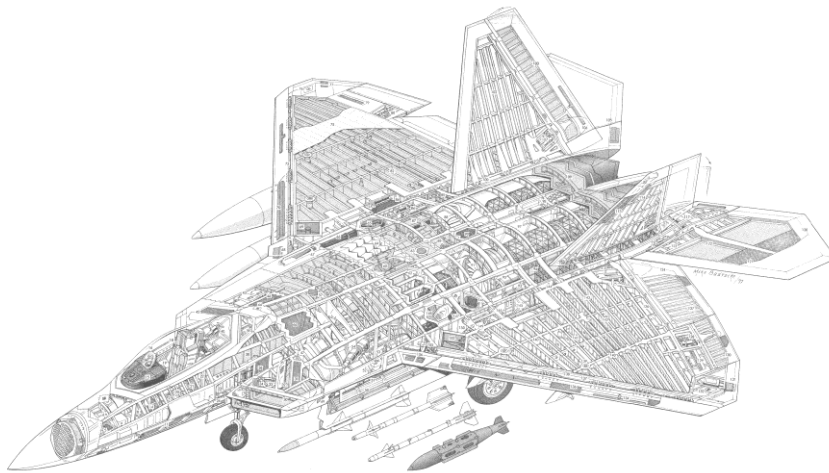


Figure 1.1 Cutway schematic



Combined with its stealth design, this makes the F35 not just a fast jet—but a force multiplier that enhances situational awareness, survivability, and mission success in contested environments [\[1\]](#).

1.2 Program History and Global Collaboration

The project, developed in the United States, began in 1994 with the JAST (Joint Advanced Strike Technology) program, which later evolved into the JSF (Joint Strike Fighter) initiative. Its primary objective was to replace multiple platforms (F-16, A-10, F/A-18, AV-8B) with a single, versatile, and interoperable aircraft.

After the Concept Exploration phase, Italy joined the Concept Demonstration phase (1996–2001) as early as 1998, which was aimed at identifying the key technologies for prototype development. In 2001, Lockheed Martin, with its X-35 prototype, was awarded the SDD (System Development and Demonstration) contract, in partnership with Northrop Grumman, BAE Systems, and Pratt & Whitney for propulsion systems. Eight nations (United Kingdom, Italy, the Netherlands, Canada, Australia, Turkey, Denmark, and Norway) participated in the development phase; additional countries such as Japan, Israel, Belgium, South Korea, Finland, Switzerland, and Germany have subsequently acquired aircraft. In Italy, the FACO (Final Assembly and Check-Out) facility in Cameri represents the only European assembly and acceptance line, serving as a strategic asset for the program and for the national industrial capability.

Table 1.1 provides a summary of legacy military aircraft replaced by the F-35 program, highlighting the operational role of each platform and the corresponding F-35 variant adopted.

Original Platform	Operational Role	F-35 Variant	Replecement Scope
F-16 Fighting Falcon 	Multirole fighter	F-35A	Full replacement for air forces
A-10 Thunderbolt II 	Close air support	F-35A (partial)	Partial CAS role integration



<p>F/A-18 Hornet</p> 	<p>Carrier-based multirole</p>	<p>F-35C</p>	<p>Full carrier-based replacement</p>
<p>AV-8B Harrier II</p> 	<p>STOVL attack aircraft</p>	<p>F-35B</p>	<p>STOVL ops for Marines and navies</p>

Table 1.1 Legacy Aircraft and Corresponding F-35 Variants

1.3 Capabilities and Evolution of the F-35 Lightning II

1.3.1 Operational Roles and Performance Profile

The F-35 is defined as an “omni-role” aircraft due to its ability to simultaneously perform multiple missions without requiring reconfiguration in flight. Its primary roles include:

- Close Air Support (CAS)
- Tactical bombing, including deep strike missions
- Air superiority, though not as specialized as the F-22 Raptor
- Air interdiction and dynamic targeting
- Support for ground-based special operations forces
- Reconnaissance and surveillance, enabled by advanced sensor fusion and stealth capabilities

The aircraft combines stealth features with high speed and agility. Its maximum speed is approximately Mach 1.6, and it can carry up to 8,160 kg of internal weaponry. The Pratt & Whitney F135-PW-100 engine delivers a thrust of approximately 191 kN. In terms of maneuverability, the F-35 has demonstrated turn rates between 20 and 30 degrees per second, along with an excellent thrust-to-weight ratio that allows it to compete with previous-generation fighters such as the F-16 and Su-30MKI, despite not being the fastest aircraft overall. During training exercises such as Red Flag 2017, the F-35 achieved exceptional

results, with a kill ratio of 20 to 1, clearly demonstrating its superiority in simulated combat scenarios compared to other fighter jets [2].

1.3.2 Upgrades and Future Development

In parallel with new procurement efforts, the F-35 is currently undergoing both a substantial technical and engineering upgrade—aimed at improving performance and extending operational life—and a series of training campaigns to expand its deployment in future high-intensity conflict scenarios. Regarding the former, several components of the platform are being modernized through the Block 4 upgrade, which includes enhancements to sensor efficiency, electronic warfare systems, communications architecture, software management, and the core power unit of the Pratt & Whitney F135 engine, with the goal of increasing both thrust and endurance.

Looking ahead, the F-35 is expected to undergo further development with the Block 5 upgrade, which will focus on a major revision of the integrated cooling system to manage the elevated thermal loads caused by the aircraft's increasingly power-hungry onboard systems.

1.4 F-35 Variants and Configurational Overview

The three variants of the aircraft — F-35A (CTOL), F-35B (STOVL), and F-35C (CATOBAR) — share over 70 % of their components, including the Pratt & Whitney F 135 engine, common avionics suite, flight-control software, and a modular airframe design. This standardization offers economies of scale, streamlined maintenance and training across allied forces, and enhanced joint interoperability in complex operations.

F-35A

This conventional take-off and landing model is optimized for traditional air force missions, replacing aircraft like the F-16 and A-10. It achieves top speeds of Mach 1.6 and a combat radius of over 590 nautical miles ($\approx 1,093$ km) on internal fuel. The inclusion of an internal GAU-22/A 25 mm cannon, boom aerial refueling, stealth profile, and internal weapons bay storing AMRAAM and GBU-31 munitions enhances survivability and mission flexibility.

F-35B

Unique to this variant is the Rolls-Royce LiftSystem, a shaft-driven lift-fan delivering roughly 20,000 lbf of cold thrust, combined with a swiveling exhaust nozzle and roll posts to provide

over 41,900 lbf of vertical lift. It can perform short take-off runs (≈ 91 m) and vertical landings while retaining supersonic capabilities, despite a reduced internal fuel capacity and combat radius (~ 833 km).

F-35C

Designed for U.S. Navy carrier operations, the F-35C features enlarged, foldable wings (13.1 m span) and reinforced landing gear capable of handling catapult-assisted takeoffs and arrested landings. With increased internal fuel, it achieves a combat radius of approximately 1,200 km, while preserving full stealth and avionics parity with the other variants.




Variant	Primary Role	Key Features	
F-35A(CTOL)	Take-off and landing(Air Force use)	Cannon, boom refueling, internal AMRAAM/GBU-31	
F-35B(STOVL)	Short take-off and vertical landing(Marine/expeditionary use)	Rolls-Royce LiftSystem	
F-35C(CATOBAR)	Carrier-based operations (Navy use)	Enlarged foldable wings, reinforced gear	

Table 1.2 Comparative Overview of F-35 Variants

As of 2023, over 960 aircraft have been delivered, accumulating more than 703,000 flight hours. By 2025, the fleet is expected to reach 1,170 aircraft with over 1 million flight hours.

2. OpenVSP

OpenVSP (Open Vehicle Sketch Pad) is a parametric aircraft geometry tool that allows users to create a 3D model of an aircraft defined by common engineering parameters. These models can then be processed into formats suitable for engineering analysis, such as aerodynamic simulations or structural evaluations.

It is the successor to earlier software tools developed by J.R. Gloudemans and others for NASA in the early 1990s, including VSP and Rapid Aircraft Modeler. These tools were part of NASA's broader initiative to support early-stage aircraft design with accessible, flexible digital modeling platforms. In January 2012, OpenVSP version 2.0 was officially released as an open-source software project, developed by Rob McDonald and distributed under the NOSE (NASA Open Source Agreement) license, making it freely available to the public.

Users can begin with predefined parametric shapes such as wings, fuselages, pods, and then proceed to more complex components like propellers, inlets, ducts, or control surfaces. These components can be adjusted and configured through an extensive set of geometric and physical parameters, making the platform particularly suitable for early design exploration and trade studies.

Moreover, OpenVSP includes a suite of embedded tools to support preliminary aerodynamic and structural analysis. Among these, one of the most powerful is VSPAERO, a solver based on vortex lattice and panel methods that allows users to perform flow simulations, stability analysis, and control surface evaluations directly from the OpenVSP geometry. Other important modules include CompGeom and DegenGeom, which prepare the geometry for numerical solvers by intersecting components and generating triangulated or simplified meshes.

2.1 VSPAERO

VSPAERO is an advanced aerodynamic analysis code developed by NASA and integrated into OpenVSP, representing an evolution of the Vortex Lattice Method (VLM). While

retaining the fundamental VLM concept, discretizing lifting surfaces using vortex elements, VSPAERO incorporates significant enhancements:

- it employs vortex rings instead of classical horseshoe vortices, yielding more accurate modeling of fluid–structure interactions [3];
- it supports geometries with finite-thickness panels, moving beyond thin-lifting-surface assumptions [4];
- it integrates linearized compressibility effects (via Prandtl–Glauert correction) [4];
- it dynamically models wake through iterative repositioning of vortex filaments along actual streamlines [5];
- it solves the resulting linear system using a GMRES iterative solver, enhanced by mesh agglomeration and parallel processing [6].

Thanks to these advancements, VSPAERO achieves higher numerical fidelity than classic VLM implementations, while maintaining computational efficiency suited for early-stage aerodynamic analysis and conceptual design workflows.

2.1.1 Core Features and Vortex Theory Foundation

VSPAERO discretizes lifting surfaces using vortex loops defined on surface panels. These panels are typically triangles or quadrilaterals, although polygons with more sides are supported. Each vortex ring consists of four vortex segments forming a closed loop, better representing flow continuity and induced velocities.

The vortex ring model is grounded in the Biot–Savart law, which expresses the velocity induced by a vortex filament at a given point in space. For a vortex segment with strength Γ between points 1 and 2, the induced velocity at point P is given by:

$$\vec{v} = \left(\frac{\Gamma}{4\pi} \right) \int \frac{\vec{R} \times d\vec{s}}{|\vec{R}|^3}$$

Here, \vec{R} is the vector from the vortex element to the field point, and $d\vec{s}$ is the differential element along the vortex segment. For compressible flows, a correction factor $\beta = \sqrt{1 - M^2}$ is applied to account for linearized compressibility effects.

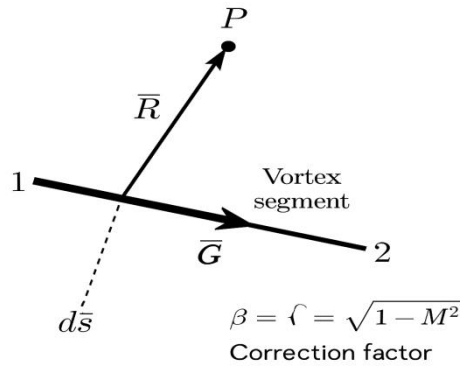


Figure 2.1 Vortex segment

2.1.2 Surface Tangency Condition and Linear System

In VSPAERO, one of the fundamental boundary conditions is the surface tangency requirement. This condition states that the net velocity vector at each control point—located typically at the center of every surface panel—must lie entirely within the tangent plane of the panel. Physically, this ensures that the flow does not penetrate the solid surface of the aircraft, which would violate the assumption of an impermeable boundary in inviscid flow theory.

Mathematically, the tangency condition is written as:

$$[\vec{V}_\infty + \vec{V}_{induced}] \cdot \hat{n} = 0$$

Here, \vec{V}_∞ represents the freestream velocity vector, $\vec{V}_{induced}$ is the velocity induced at the control point by all other vortex rings and trailing wakes, and \hat{n} is the unit normal vector to the surface at that control point. By enforcing this condition on every panel, VSPAERO constructs a system of linear equations where the unknowns are the circulation strengths (Γ) of the vortex rings:

$$A \Gamma = b$$

In this equation, A is the influence coefficient matrix which quantifies the velocity induced at each panel due to every other panel's vortex strength, Γ is the vector of unknown circulations, and b contains the components of the freestream velocity projected in the normal direction. To ensure a physically accurate flow separation at trailing edges, the solver imposes the Kutta

condition. This condition ensures that the flow departs smoothly from the trailing edge, avoiding unrealistic pressure spikes or flow reversal.

2.1.3 Iterative Solver and Preconditioning

Solving the linear system $A\Gamma = b$ directly can become computationally expensive, especially for high-resolution models that use thousands of panels. In such cases, VSPAERO employs the Generalized Minimal Residual (GMRES) iterative solver. GMRES operates by progressively reducing the residual vector $R = b - A\Gamma$, with the goal of finding a solution Γ that drives this residual to near-zero.

To enhance convergence speed and numerical stability, preconditioning techniques are used. A preconditioner modifies the linear system into an equivalent but numerically better-conditioned form.

By preconditioning the system, GMRES can converge more rapidly, particularly when dealing with large sparse matrices that arise from detailed aerodynamic models. This enables users to perform high-fidelity simulations without prohibitive computational costs.

2.1.4 Computational Complexity and Fast Multipole Strategy

The induced velocity computation between all vortex loops is inherently $O(N^2)$. VSPAERO implements a fast multipole-like algorithm to reduce the complexity to approximately $O(N \log N)$ by grouping distant vortices and approximating their collective influence as a single entity.

2.1.5 Wake Modeling and Streamline Adaptation

Trailing wakes are initially generated as straight filaments aligned with the freestream. As the solution converges, their geometry is updated to follow actual streamlines according to:

$$dx/ds = u/q, dy/ds = v/q, dz/ds = w/q$$

where u , v , and w are the velocity components and q are the total velocity magnitude. This ensures a physically realistic representation of wake behavior in steady flight.

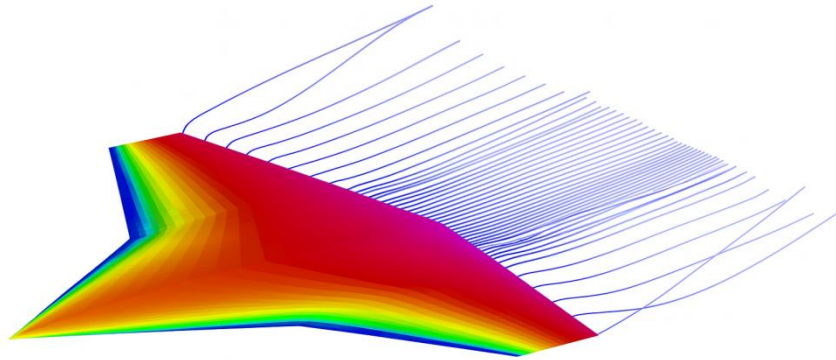


Figure 2.2 Curved Wake Lines from VSPAERO

In the outermost regions of the wing, the trailing wakes curve due to the generation of tip vortices. These are caused by pressure differentials between the upper and lower wing surfaces, leading to spanwise flow and vortex roll-up at the wingtips. The resulting wake deformation reflects the physics of induced drag and circulation.

3. Geometric modelling of the F-35A Lightning II

The F-35A Lightning II aircraft shown in Figure 3.1 will be analyzed in this chapter. The aircraft has been geometrically modeled in OpenVSP.

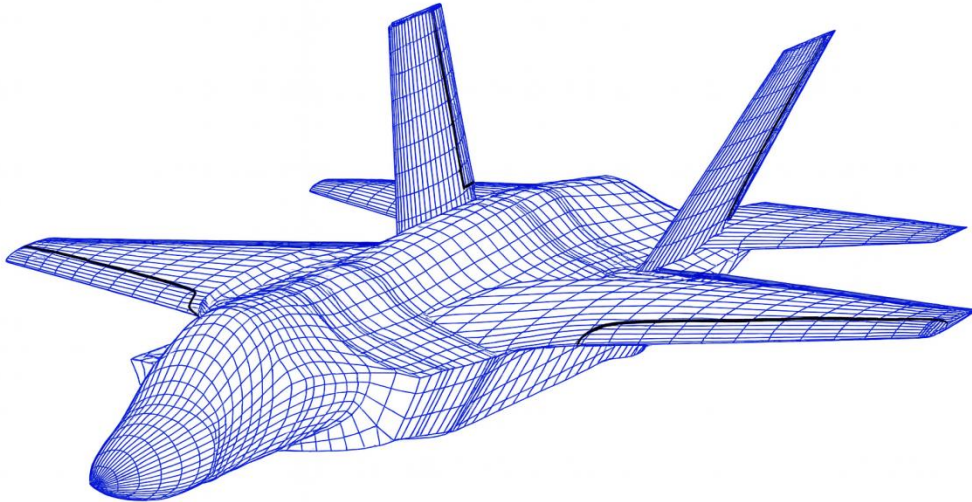


Figure 3.1 an F-35A model in Open VSP

The model's dimensions were derived from manuals, photographs and reference images. Specifically, the aircraft's three-view drawing was sourced from Wikipedia.

3.1 Fuselage

The fuselage was the most complex part of the aircraft to model. To obtain reliable data regarding its dimensions, the top view of the F-35A was used as a reference. In this view, the wingspan is known to be approximately 10.7 meters. Measurements were taken while maintaining the correct scale ratio. The resulting length spans from the nose of the fuselage to the junction with the horizontal stabilizer.

By entering these values into the Design Panel, a cylindrical base shape is generated, which is then refined by defining the length and width of each cross-section. The views used for this process were the top and side views. Figure 3.2 shows the preliminary process of measuring the fuselage dimensions and its alignment with the three-view drawing.

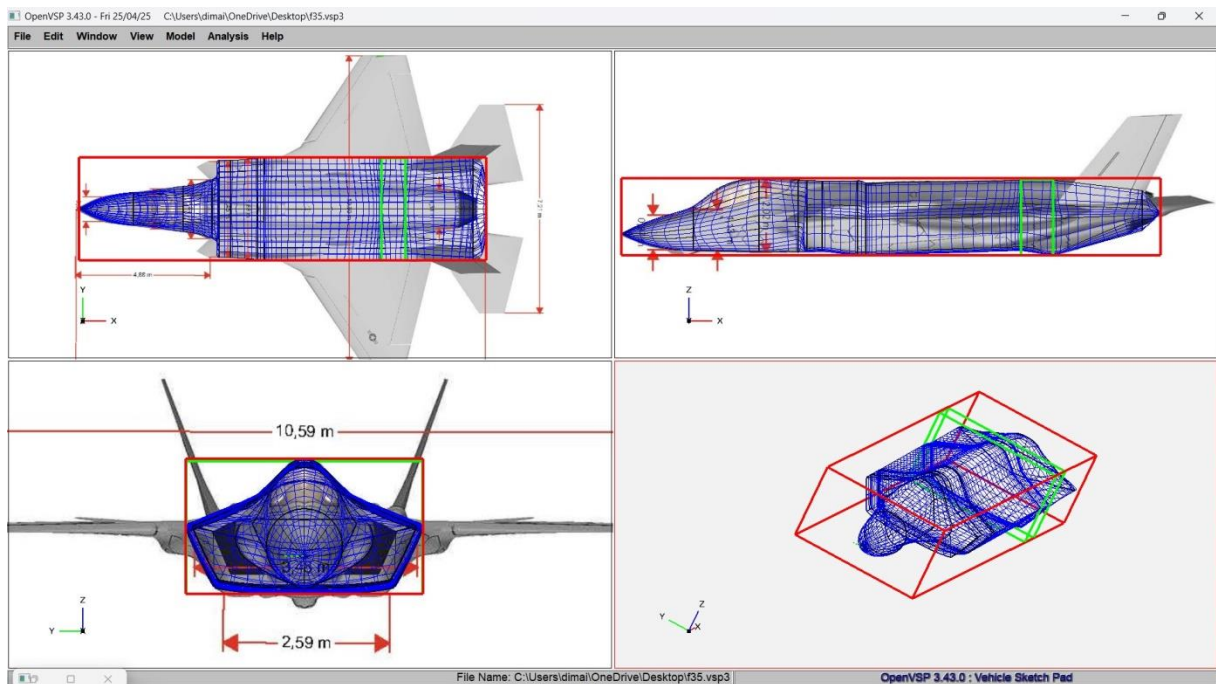


Figure 3.2 Alignment of the modeled fuselage with the orthogonal three-view of the F-35A in OpenVSP

Subsequently, in the Skinning Panel, the longitudinal profile of the aircraft can be modeled by defining and refining the shape of the surfaces between the various cross-sections. Finally, as the last step, the desired cross-sectional shapes are defined using the Edit Curve command, which allows either the selection of a predefined geometry or the creation of a custom one, as was the case for the modeled aircraft.

By adjusting the control points and visualizing the Bezier curve (in green), it is possible to define the desired geometry for each section by varying parameters such as width, height, and depth, and manually modifying the position of individual nodes, as shown in Figure 3.3. Moreover, if aerodynamic analysis is to be carried out using the VLM (Vortex Lattice Method), it is essential to avoid perfectly vertical or horizontal surfaces on the fuselage. Such configurations may degenerate into cruciform geometries where some lines of the computational mesh overlap, potentially invalidating the calculation results or even causing the software to crash.

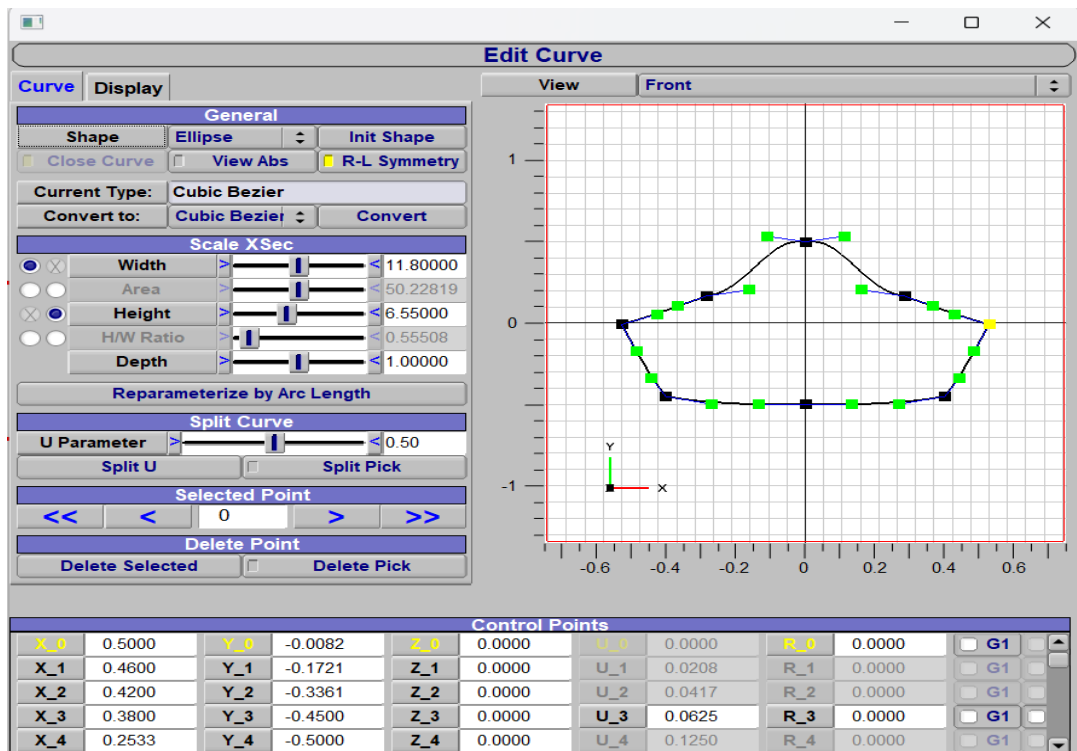


Figure 3.3 OpenVSP “Edit Curve” panel applied to the fuselage cross-section

3.2 Wing

The wing modeled for the F-35A aircraft features a trapezoidal planform with moderate leading-edge sweep and no appreciable dihedral, with a total span of approximately 10.7 m. Although some sources report a dihedral angle of about 1° , it is effectively negligible and can be treated as zero in modeling applications such as OpenVSP. This design choice is consistent with the aircraft’s stealth configuration and fly-by-wire controlled aerodynamic stability.

Since the real wing profile is unknown, the selected airfoil is the NACA 64A210, a laminar flow profile belonging to the 6-series family, as shown in Figure 3.4. This type of airfoil was chosen for its ability to delay boundary layer transition and reduce drag, characteristics consistent with the aerodynamic requirements of high-speed, low-observability fighter aircraft. The airfoil data was imported directly from the Airfoil Tools database (airfoiltools.com) using the coordinate file available in the public Airfoil Database list, and then uploaded into OpenVSP via a .dat file to ensure geometric accuracy.

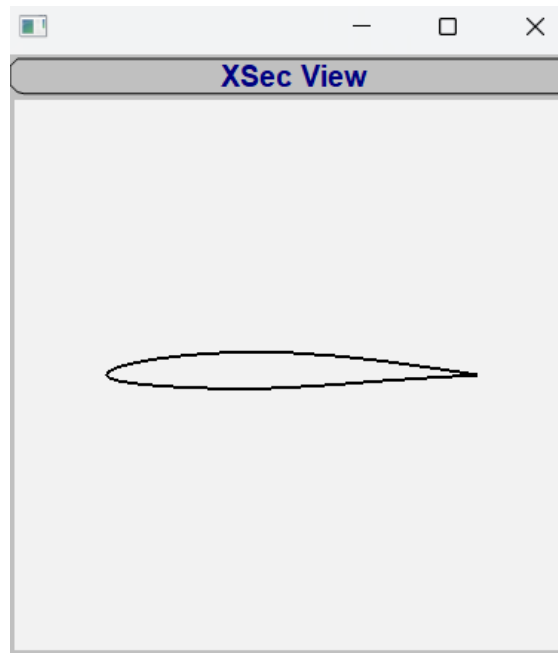


Figure 3.4 Cross-sectional view of the NACA 64A210 airfoil

Control surfaces, including flaps and ailerons, were integrated into the wing geometry using the 'Sub' feature in OpenVSP. This tool allows for the definition of sub-surfaces directly on the parent surface by drawing their boundaries interactively, without the need to create them as independent components. This approach is particularly efficient for preliminary design and aerodynamic analysis, as it simplifies the modeling process while retaining geometric coherence with the main lifting surface.

Although these sub-elements do not influence the structural model or mesh directly, they are recognized in aerodynamic solvers like VSPAERO, which interprets them as movable control surfaces, enabling detailed analysis of control effectiveness and stability derivatives. This method is especially advantageous in conceptual design phases, where speed and flexibility in testing different configurations are essential. In the case of the F-35A wing, the inclusion of control surfaces using this strategy provided a practical way to replicate the aerodynamic behavior of the real aircraft while maintaining a manageable model complexity, as shown in Figure 3.5.

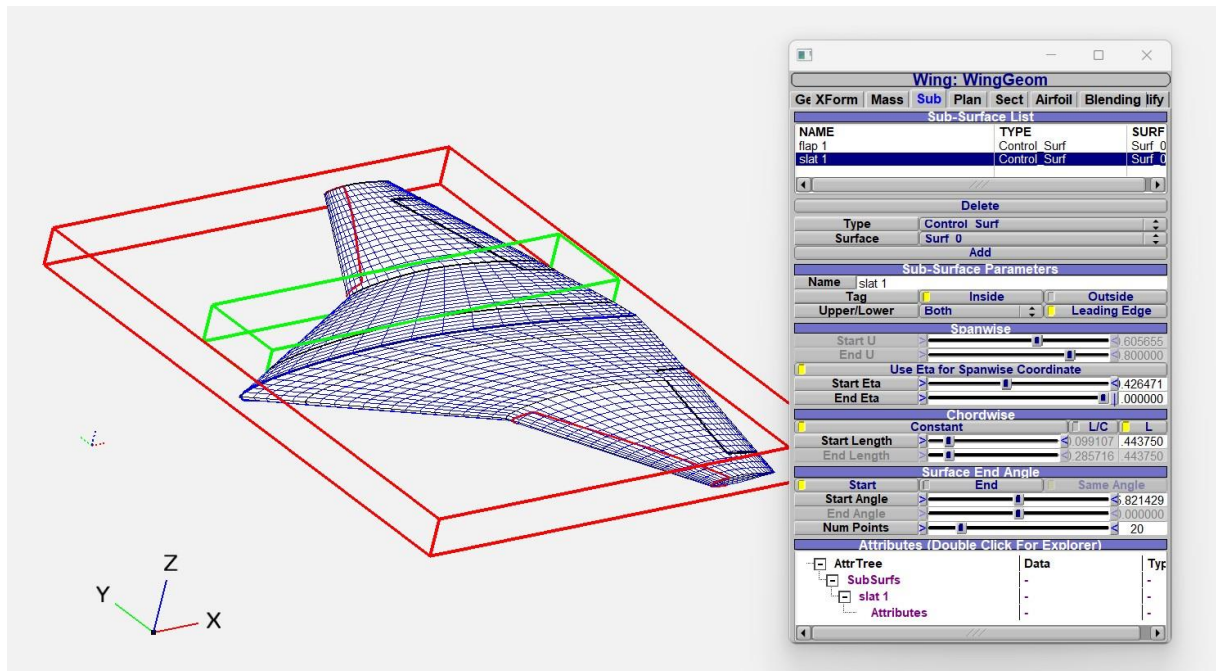


Figure 3.5 Control surfaces

3.3 Horizontal stabilizer

The modeling of the horizontal stabilizer followed the same approach used for the main wings: in this case as well, the geometry was derived from the three-view drawings of the F-35A. For this reason, in the resulting model, the stabilator appears to be partially embedded into the fuselage, as the outlines were traced faithfully based on the available orthographic projections.

In the case of the F-35A aircraft, the horizontal tailplane is not divided into a fixed and a movable part, as is typical in conventional stabilizers with an elevator. Instead, it consists of a fully movable stabilator (all-moving horizontal tail). This configuration, adopted in many modern fighter jets, provides greater pitch control authority and more effective maneuvering response, especially at high speeds.

To accurately represent this component in OpenVSP, the Hinge function was used, which allows the definition of a rotation axis around which an aerodynamic surface can move. Specifically, the hinge was attached directly to the fuselage, and a wing element was then connected to it, acting as the movable stabilator. This wing is free to rotate around the hinge,

thus simulating the actual deflection of the stabilator during flight. Figure 3.6 illustrates this configuration in the final model.

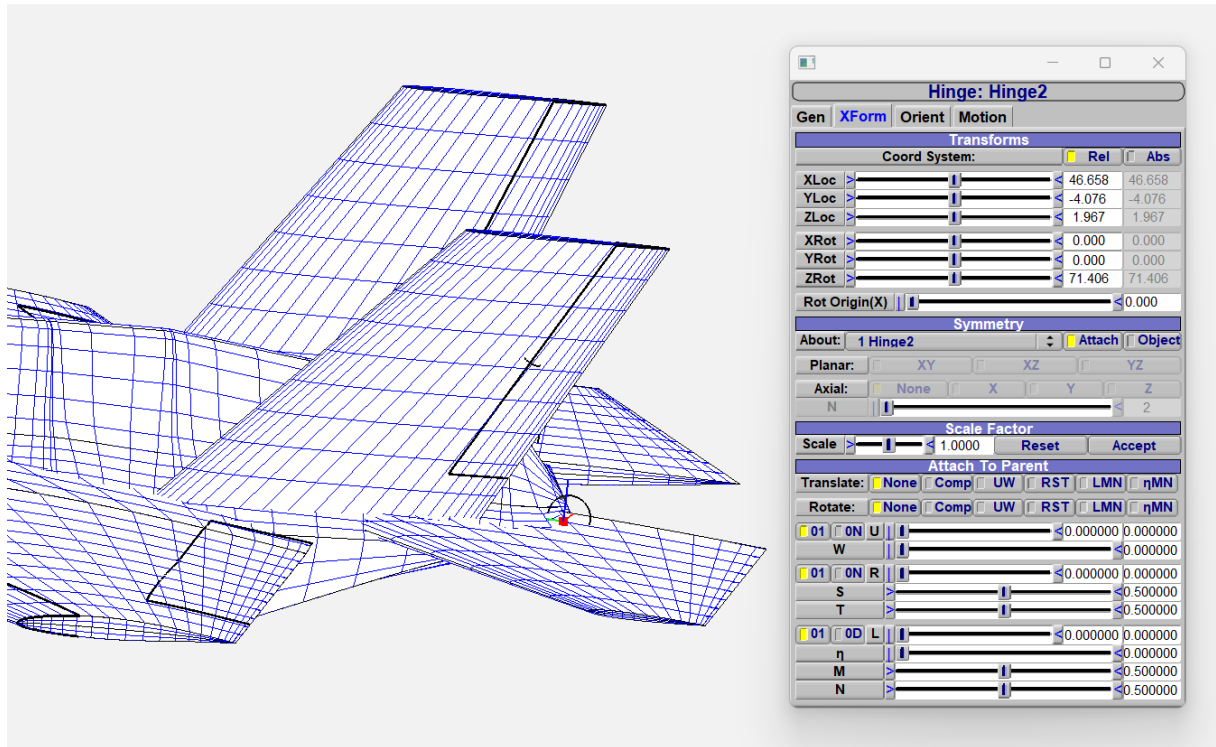


Figure 3.6 Configuration of the horizontal stabilator hinge in OpenVSP, showing rotation parameters and attachment to the fuselage

Finally, just as for the vertical tail, the NACA0010 airfoil was selected for the horizontal stabilator. This symmetric airfoil is commonly used for control surfaces due to its balanced aerodynamic behavior and its ability to generate forces effectively in both positive and negative deflection angles, ensuring responsive and stable pitch control

3.4 Vertical stabilizer

The F-35A features a pair of twin vertical stabilizers, arranged symmetrically with respect to the aircraft's longitudinal axis. This configuration differs from traditional single-fin tails, offering both stealth advantages and enhanced maneuverability. One of the key characteristics of these vertical surfaces is their dihedral angle, meaning they are outwardly canted rather than perfectly vertical. This design choice contributes to aerodynamic stability at high angles of attack and helps to reduce the aircraft's radar cross-section, aligning with the stealth requirements of fifth-generation fighters.

In OpenVSP, the vertical tail was modeled as a single wing component, properly rotated to match the cant angle, and the symmetry option was activated to automatically generate the mirrored counterpart. A dihedral angle of 79 degrees was applied to reflect the actual inclination of the stabilizers and to reproduce their aerodynamic effect within the model.

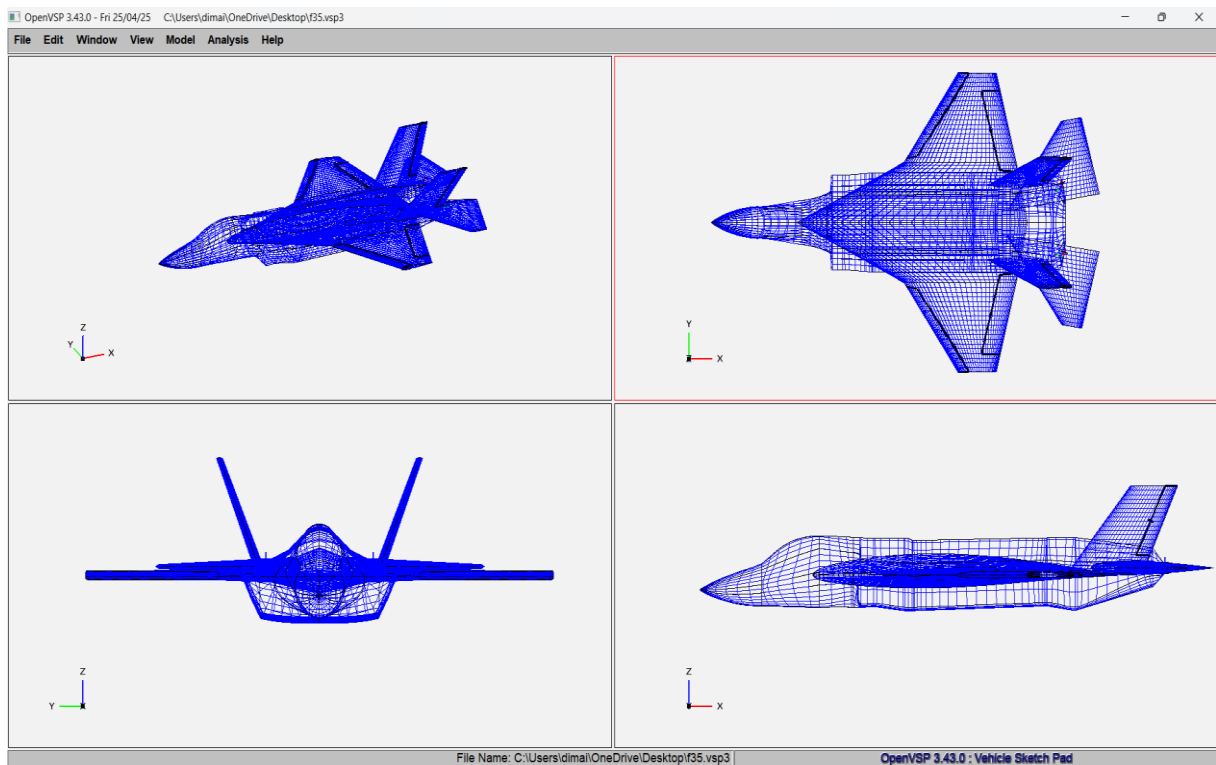


Figure 3.7 Complete aircraft: mesh visualization

4. Longitudinal Aerodynamics Analysis

This section presents the results of the longitudinal stability and control analysis performed on the F-35 fighter aircraft using the VSPAERO solver. As introduced in Chapter 2, the Vortex Lattice Method (VLM) was selected for this analysis due to its suitability for modeling lifting surfaces under incompressible, inviscid flow conditions. Compared to the Panel Method, VLM offers lower computational cost and faster simulations, making it more appropriate for early-stage aerodynamic evaluations, especially when thickness and flow separation effects are not dominant. Symmetry with respect to the X–Z plane was enabled, which also justified setting the sideslip angle (β) to zero throughout the simulation.

The aircraft model provided the key geometric reference parameters, including the planform area (S), wingspan (b), mean aerodynamic chord (c), and the center of gravity location, so the parameters related to the *Reference Area* are set to "From model", allowing the software to automatically compute the values of S_{ref} , b_{ref} , and c_{ref} .

4.1 Lift coefficient curves

4.1.1 Clean configuration

The flow conditions were initialized with a Mach number of 0.4 and a Reynolds number of 2.4×10^8 . The angle of attack (α) was varied from -8° to $+20^\circ$ while keeping the values of β , Mach, and Reynolds constant. Additionally, in this initial analysis, all control surfaces are kept in the neutral position (0°). Running the solver, VSPAERO collects the data in text files, which have been processed in Excel.

It is important to point out that VSPAERO cannot simulate stall conditions, therefore only the linear portion of the lift coefficient curves is considered.

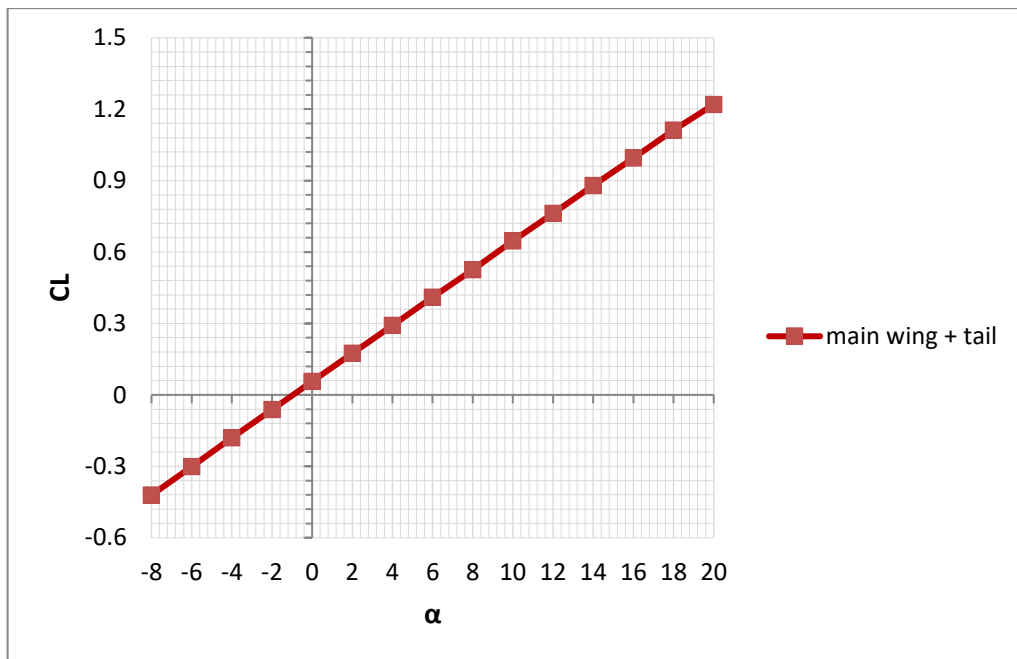


Figure 4.1 Lift curve C_L vs α for the clean wing + tail configuration

The graph in Figure 4.1 shows that the lift coefficient increases as the angle of attack increases, as expected. We can mathematically confirm this increase in the slope of the curve by using the Excel SLOPE function, which calculates the following aerodynamic derivative: $C_{L\alpha} = 0.05874\text{deg}^{-1}$.

4.1.2 Effect of Control Surface Deflections on Lift Characteristics

In the following section, the effects of control surface deflections on the wing, specifically flaps, are analyzed in relation to the lift coefficient. Subsequently, the control derivative is investigated, namely the variation of C_L as a function of the deflection of the all-moving horizontal tails (stabilators) of the F-35. Figure 4.2 illustrates the impact of wing flap deflections on the aircraft's lift coefficient C_L .

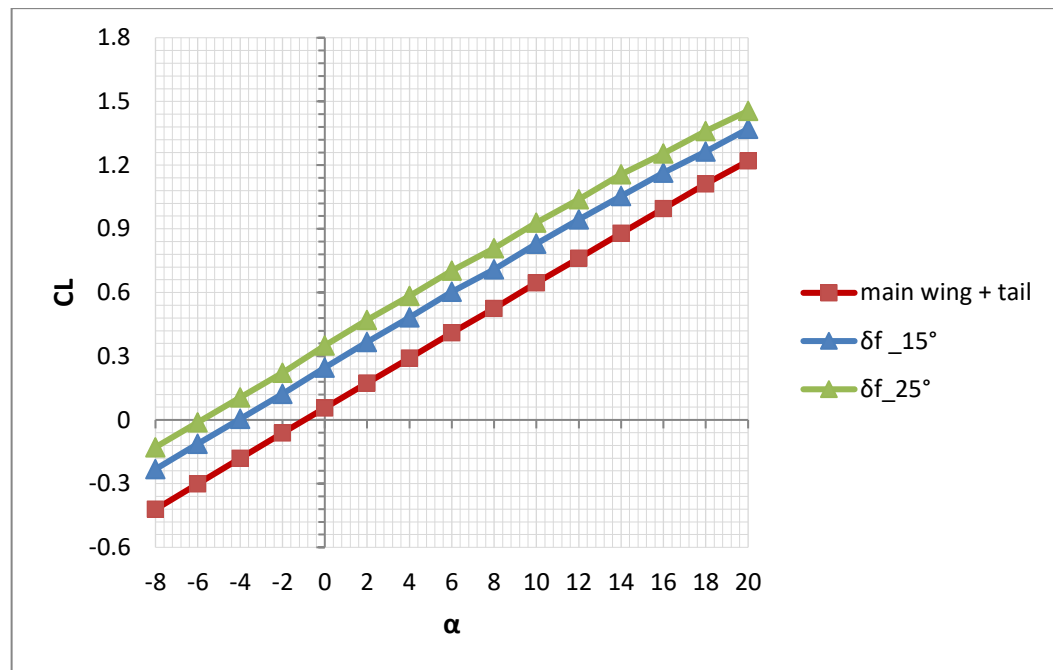


Figure 4.2 Effect of wing flap deflection on lift coefficient

To assess the effectiveness of the horizontal stabilizer in controlling lift, the control derivative $dC_L/d\delta_s$ was analyzed. This derivative quantifies the variation of the lift coefficient C_L as a function of the stabilizer deflection angle δ_s .

For this purpose, the angle of attack was held constant at $\alpha = 0^\circ$ to isolate the effect of the stabilizer deflection alone. A series of aerodynamic simulations were performed by systematically varying δ_s within a symmetric range, typically from -10° to $+10^\circ$.

In each simulation, the deflection of the horizontal stabilizer was implemented by manually modifying the stabilizer geometry in OpenVSP. This ensured that the new orientation of the surface was accurately reflected in the aerodynamic model. For each configuration, the corresponding total lift coefficient of the aircraft was recorded. The resulting C_L values were then plotted as a function of δ_s , and a linear interpolation was applied to the data. The slope of the resulting regression line represents the value of the derivative.

This approach allows for the estimation of the horizontal stabilizer's influence on the aircraft's lift in linear flight conditions and provides a quantitative measure useful for stability and control analysis. The deflection is positive downward.

δ_s	-10°	-5°	0°	5°	10°
C_L	-0.096	-0.026	0.048	0.097	0.159

$$\frac{dC_L}{d\delta_s} = 0.0127 \text{ deg}^{-1}$$

This has physical meaning: the downward deflection of the horizontal stabilizer generates an upward force on the stabilizer, which causes the nose of the aircraft to pitch up. As a result, the angle of attack increases, leading to an increase in the total lift coefficient of the aircraft.

4.2 Pitching moment coefficient curves

4.2.1 Clean configuration

In the context of aerodynamics and flight dynamics, the pitching moment is the aerodynamic moment acting about the aircraft's lateral axis, responsible for variations in angle of attack and longitudinal attitude. It plays a central role in the analysis of static longitudinal stability as well as in the dynamic response characteristics of the aircraft [7]. The static longitudinal behavior of an aircraft is primarily governed by the sign of the partial derivative $dC_M/d\alpha$ known as the **longitudinal static stability derivative**. According to classical stability criteria, an aerodynamic system is considered **statically stable** in pitch if:

$$\frac{dC_M}{d\alpha} < 0$$

meaning that a perturbation causing an increase in angle of attack generates a negative (restoring) pitching moment, which tends to return the aircraft to its original equilibrium state [8]. Conversely, a positive derivative implies static instability, where perturbations are amplified instead of damped.

A key design consideration in ensuring longitudinal stability is the proper placement of the aircraft's center of gravity aft of the aerodynamic center, such that the resulting moment variation aligns with stability requirements [8]. This concept underlies the use and sizing of horizontal stabilizers, whose configuration plays a critical role in achieving the desired trim and stability margins [7].

The position of the center of gravity with respect to the aircraft's nose was manually defined based on estimates available from technical sources and publicly accessible literature. The exact location of the CG depends on the aircraft configuration and loading conditions, such as fuel, internal weapons, and pilot weight.

Figure 4.3 illustrates the variation of the pitching moment coefficient as a function of the angle of attack, α . The graph displays two curves corresponding to different center of gravity (CG) positions. The purple curve refers to a CG located at 57% of the fuselage length (which is 47 feet long), while the blue curve corresponds to a CG position at 45% of the fuselage length. In the following analyses, reference will be made to the configuration with the CG at 45%. The center of gravity (CG) was positioned at 22.0 ft from the nose of the fuselage. Given that the leading edge of the mean aerodynamic chord (MAC) lies at approximately 11.382 ft and the MAC length is 18.564 ft, values obtained from the DegenGeom file exported from OpenVSP, the CG corresponds to 56.32% of the MAC, measured from its leading edge.

It is important to note that the more forward the CG is positioned, the more longitudinally stable the aircraft becomes. However, this increased stability comes at the cost of reduced maneuverability. For this reason, fighter aircraft or aircraft designed to perform agile maneuvers and aerobatics often require a more aft CG position to enhance responsiveness and maneuverability in flight.

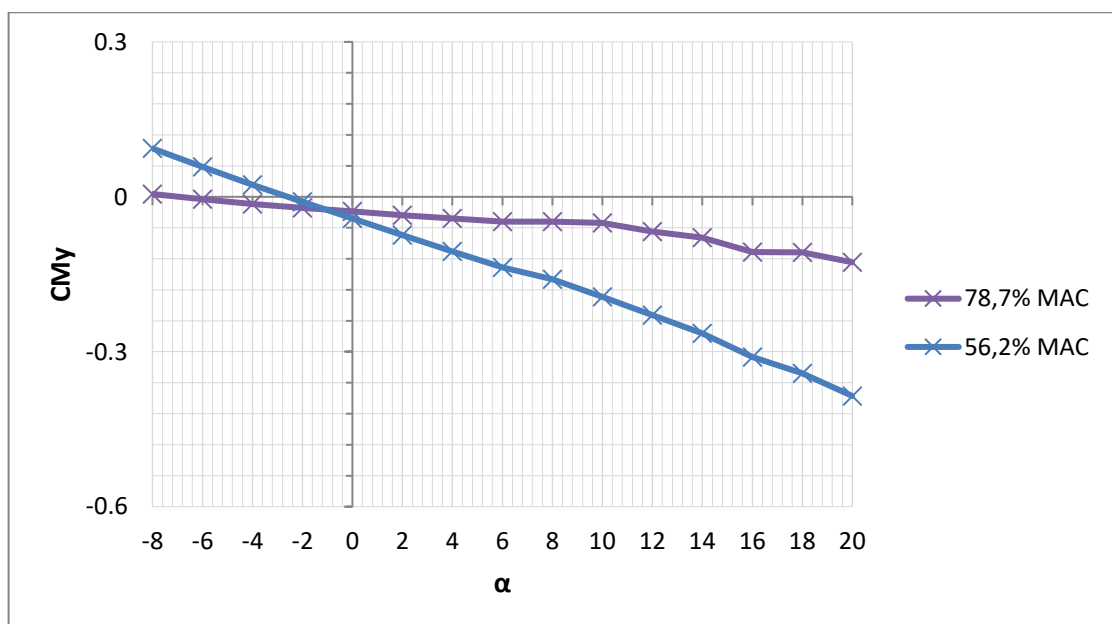


Figure 4.3 Variation of pitching moment coefficient (CM_y) with angle of attack (α) for two different CG positions

The longitudinal static stability derivative $C_{M\alpha}$ was calculated using the SLOPE function in Excel, applied to the curve of pitching moment coefficient versus angle of attack. The resulting value, $C_{M\alpha} = -0.0167 \text{ deg}^{-1}$, indicates a configuration with reduced longitudinal stability. This value, while significantly lower than that of commercial aircraft (typically between -0.05 and -0.1), is consistent with the relaxed static stability design philosophy adopted in modern fighter jets such as the F-35. Such a low negative slope ensures high maneuverability, at the cost of reduced natural stability, and is typically compensated by advanced fly-by-wire control systems.

4.2.2 Effect of control surfaces on longitudinal stability

In Figure 4.4, multiple curves of the pitching moment coefficient are presented as a function of flap deflection, in a manner analogous to the analysis previously conducted for the aircraft's lift coefficient.

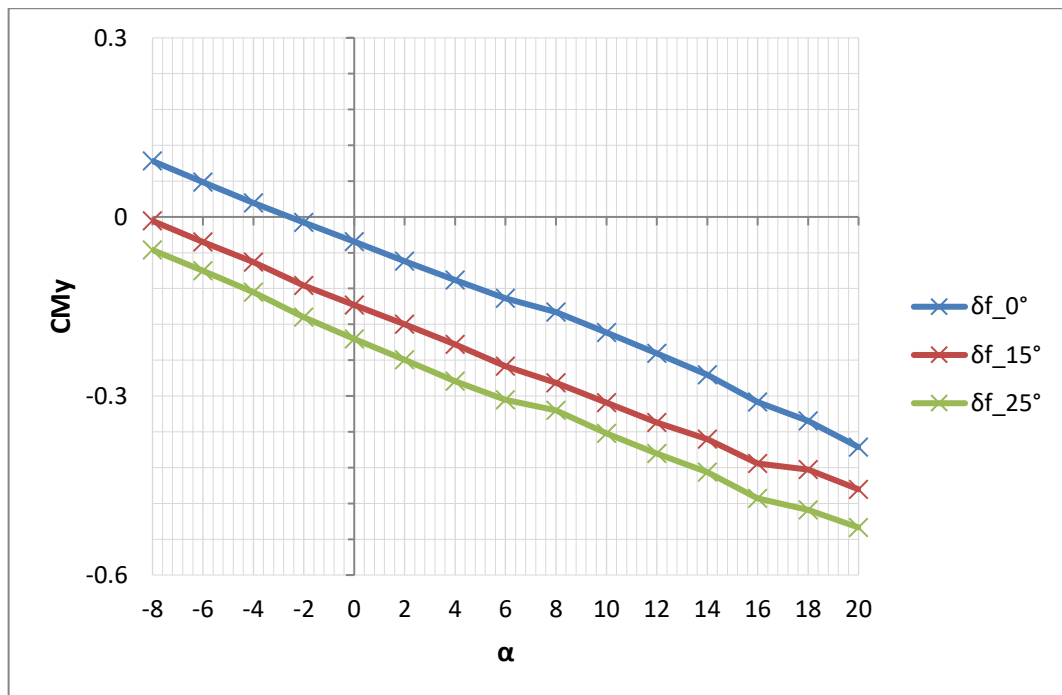


Figure 4.4 Pitching moment coefficient vs. angle of attack for different flap deflections

Increasing flap deflection results in a downward shift of the pitching moment coefficient curve across all angles of attack, due to the increased lift generated by the wing, which amplifies its nose-down pitching moment contribution.

The control derivative $dC_M/d\delta_s$, defined as the variation of the pitching moment coefficient with respect to the deflection of the all-moving horizontal stabilizer δ_s , represents the pitch control effectiveness of this surface in the case of the F-35. Physically, this derivative quantifies the amount of nose-up or nose-down pitching moment generated by a change in stabilator deflection, directly influencing the aircraft's trim capability and pitch maneuverability. In this study, $dC_M/d\delta_s$ was computed following the same procedure adopted for the lift coefficient : the aircraft geometry was progressively modified to account for different stabilator deflections, and aerodynamic analyses were carried out on each modified configuration. The resulting pitching moment coefficient values were then interpolated as a function of deflection in order to derive the control derivative.

δ_s	-10°	-5°	0°	5°	10°
C_{M_y}	0.120	0.040	-0.032	-0.109	-0.183

$$\frac{dC_M}{d\delta_s} = -0.0151 \text{ deg}^{-1}$$

As expected, positive deflections of the all-moving stabilator (downward) increase the nose-down pitching moment.

4.3 Aerodynamic Polar Analysis of the Aircraft

The lift–drag polar curve C_L-C_D describes the relationship between the lift coefficient and the total aerodynamic drag coefficient of an aircraft as a function of flight conditions. In a clean configuration—meaning all control surfaces are neutral and no high-lift devices such as flaps or slats are deployed—the polar provides a direct representation of the aircraft’s intrinsic aerodynamic characteristics under ideal conditions. This curve encapsulates how efficiently the aircraft can generate lift relative to the aerodynamic drag it experiences.

The total drag coefficient C_D is typically decomposed into two main components: the parasite drag C_{D_0} , which is independent of lift, and the induced drag C_{D_i} , which is directly related to lift production. The parasite drag arises from viscous effects and includes skin friction drag over wetted surfaces, form drag due to pressure distribution, and interference drag from the interaction of different airframe components. Induced drag, on the other hand, increases quadratically with the lift coefficient and is governed by the expression $C_{D_i} = \frac{C_L^2}{\pi e AR}$, where AR is the wing aspect ratio and e is the Oswald efficiency factor. This factor accounts for deviations from the ideal elliptical lift distribution and includes the effects of three-dimensional flow and viscous losses. For typical subsonic aircraft, e ranges from approximately 0.7 to 0.85.

The clean polar curve generally exhibits a convex parabolic shape, well approximated by the relation $C_D = C_{D_0} + kC_L^2$. The curve shown in figure 4.5 illustrates the trend of C_L - C_D in clean configuration and serves as a fundamental reference for evaluating the aerodynamic performance of the aircraft. The figure also shows the contribution of the induced drag coefficient C_{D_i} .

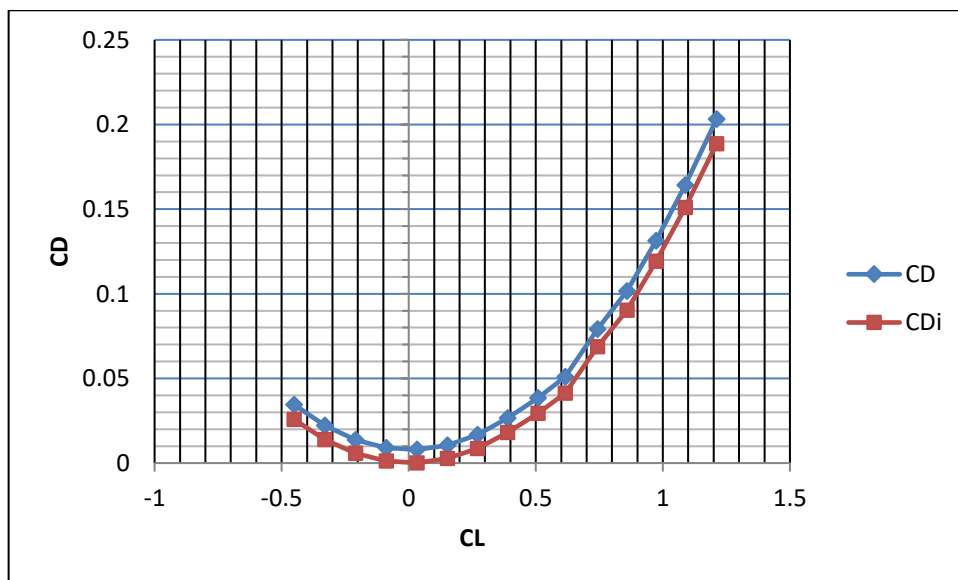


Figure 4.5 Polar curve of the aircraft in clean configuration

It might be interesting to analyze the behavior of the curve as the flap deflection varies, as shown in figure 4.6.

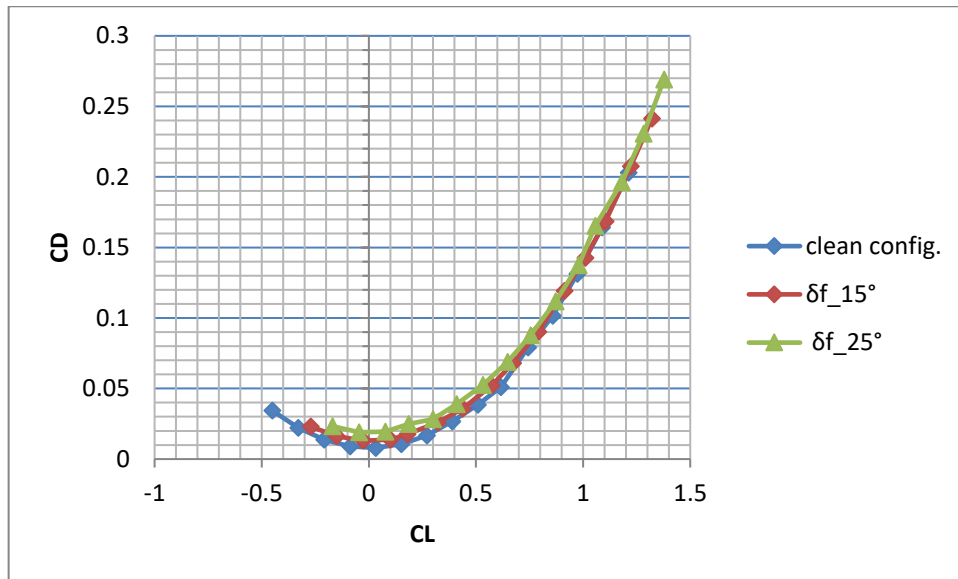


Figure 4.6 Drag polar for clean and deflected flap configurations

Flap deflection increases the camber of the airfoil, resulting in a higher lift coefficient at a given angle of attack. This effect is accompanied by an increase in both parasite and induced drag, shifting the drag polar upward and slightly to the left. The overall result is a reduction in aerodynamic efficiency (L/D), but an improved lift capability at low speeds, which is beneficial during takeoff and landing.

The increase in total drag is primarily due to the induced component, as Vortex Lattice Methods (VLM), such as those implemented in VSPAERO, are well-suited for predicting induced drag. However, the estimation of parasite drag relies on semi-empirical correlations included in VSPAERO, which often tend to underestimate this contribution. As a result, while the induced drag variation due to flap deflection is captured with reasonable accuracy, the total drag may be slightly underpredicted, especially at lower speeds where flap deployment is more significant.

5. Lateral and Directional Aerodynamics Analysis

As in the case of longitudinal stability analysis, the behavior of the aircraft in the lateral-directional domain is studied by linearizing the equations of motion around an equilibrium point, typically corresponding to steady, level flight. In this regime, aerodynamic forces and moments can be expressed as linear functions of the state variables and control surface deflections. The coefficients that appear in these expressions are known as aerodynamic stability and control derivatives, and they quantify the sensitivity of the aircraft to small perturbations about the trim condition.

In the lateral-directional domain, the relevant aerodynamic coefficients are:

- C_Y : side force coefficient, responsible for lateral translation along the body Y-axis;
- C_{M_z} : yawing moment coefficient, related to rotation about the vertical (Z) axis;
- C_{M_x} : rolling moment coefficient, associated with rotation about the longitudinal (X) axis;

From the relations linking these coefficients to the states and control inputs, the corresponding derivatives arise, each with a well-defined physical meaning. These derivatives indicate how strongly a specific variation (in state or control input) influences the generation of aerodynamic forces or moments.

For lateral-directional stability and control analyses, the CG is set in the same position used for longitudinal analyses. In this case, symmetry along the X-Z plane is deactivated. Alpha is set to 0° , Mach and Reynolds numbers remain constant, while β varies between -8° and 20° . It is important to highlight that VSPAERO does not use the Body Reference Frame but instead employs the Construction Reference Frame (CRF), where the X-axis points aft, the Y-axis points toward the right wing, and the Z-axis points upward as represented in figure 5.1. Clearly, the origin of the reference frame is still the center of gravity. Although this distinction has no effect on pitch dynamics, it does impact the interpretation of roll and yaw behavior. Specifically, the resulting plots may seem inconsistent with conventional lateral-directional stability criteria, where a stable configuration is typically associated with a negative C_{M_x} (roll moment coefficient) and positive C_{M_z} (yaw moment coefficient). However, this apparent contradiction arises from the use of the body-axis coordinate system (CRF), in

which the signs of these derivatives are inverted. As a result, positive C_{M_x} and negative C_{M_z} in this reference frame actually indicate a statically stable response in roll and yaw, respectively.

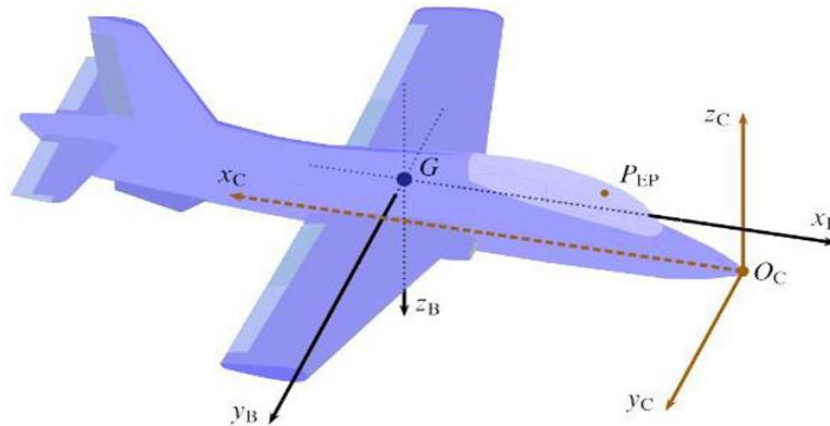


Figure 5.1 Body Reference Frame and Constructive Reference Frame

It is important to emphasize that, unlike in longitudinal stability analysis, where both flaps typically deflect in the same direction to increase or decrease lift symmetrically, in lateral-directional analysis the flaps are deflected by equal magnitude but in opposite directions. This is achieved by setting the deflection gains to $(1, 1)$, as illustrated in Figure 5.2, ensuring that the surface normals of the left and right flaperons rotate in opposite directions.

Current Control Surface Group Details	
Group Name	wing flap
Deflection Gain per Surface	
WingGeom_Surf0_flap 1	1.00
WingGeom_Surf1_flap 1	1.00

Figure 5.2 Flap Deflection Gain

5.1 Sideforce coefficient C_Y

Initially, the variation of the lateral force coefficient with respect to the sideslip angle is analyzed, considering both the clean configuration and multiple antisymmetric flaperon deflection settings as shown in figure 5.3.

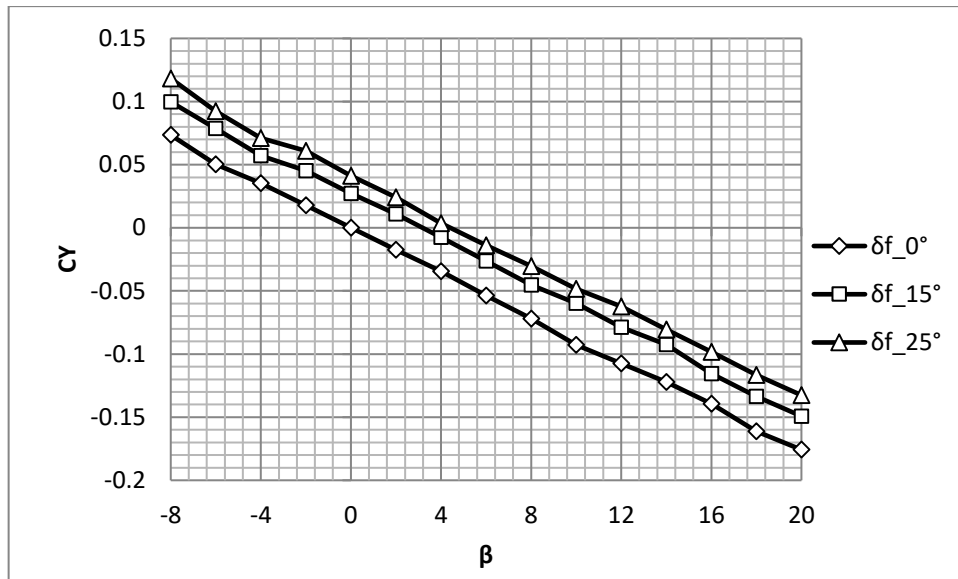


Figure 5.3 C_Y vs. β with antisymmetric variations of $\delta_f = 0^\circ, 15^\circ, 25^\circ$

The curve illustrates the behavior of the lateral force coefficient C_Y as a function of the sideslip angle β . When β is positive, the relative wind comes from the right. In this condition, the airflow strikes the vertical tail surface at an angle, generating an aerodynamic force (lift) directed to the left. This lateral force, which is more significant than that generated by the fuselage or wings, is primarily responsible for producing a yawing moment that turns the aircraft nose into the wind, thus decreasing the sideslip angle. This is a stabilizing mechanism: the aerodynamic moment tends to restore equilibrium by aligning the aircraft with the relative wind. The negative slope of the curve $dC_Y/d\beta$ reflects this directional stability.

The stability derivative was obtained using the SLOPE function in Excel in the β range where the aerodynamic coefficient exhibited a linear trend: $\frac{dC_Y}{d\beta} = -0.0089 \text{ deg}^{-1}$.

Given that the vertical tail is the primary contributor to the lateral force generated under sideslip conditions, it is particularly relevant to investigate the variation of the lateral force coefficient as a function of rudder deflection δ_r . In the case of rudder deflection, the effective angle of attack experienced by the vertical tail becomes a quantity approximately proportional to the rudder deflection itself, resulting in a corresponding variation in the generated lateral aerodynamic force. Figure 5.4 shows the trend of the lateral force coefficient as a function of the sideslip angle β for rudder deflections of $0^\circ, 10^\circ, 20^\circ$, and 30° .

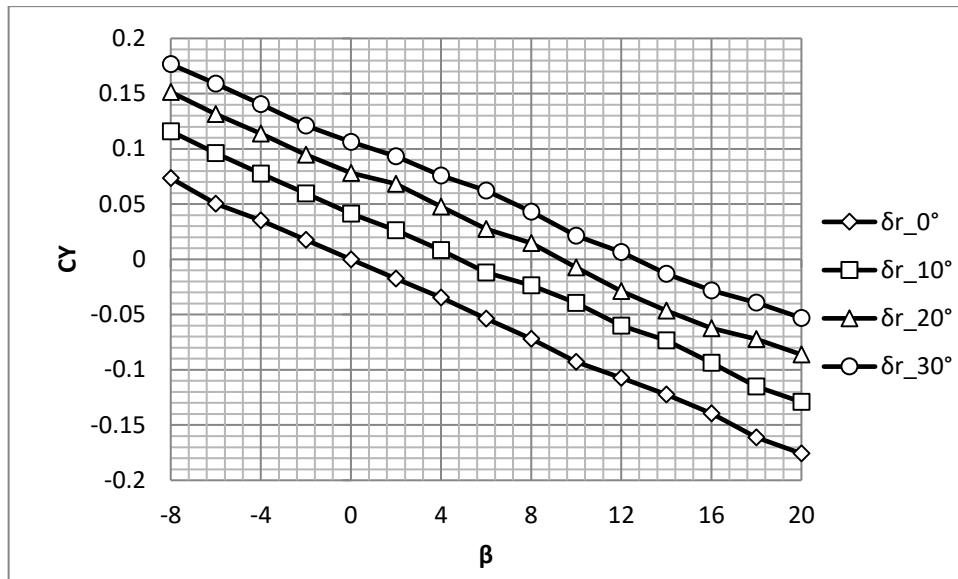


Figure 5.4 Side force coefficient C_Y vs. β for different rudder deflections δ_r

The graph illustrates the variation of the side force coefficient C_Y with respect to the sideslip angle β , for different rudder deflections δ_r . A nearly linear decreasing trend is observed: as the sideslip angle increases, C_Y becomes more negative, indicating the generation of a lateral force opposite to the aircraft's motion. This behavior is typical of a directionally stable configuration.

The effect of rudder deflection is clearly visible: for a given β , increasing δ_r results in a stronger lateral force, with the corresponding C_Y curves shifting downward. This is consistent with classical flight dynamics theory, where the rudder is used to enhance directional control and trim under asymmetric flight conditions or during coordinated maneuvers [9].

To estimate the control derivative, the Excel SLOPE function was used, based on the values of the aircraft's side force coefficient corresponding to zero sideslip angle and the rudder deflections previously plotted.

δ_r	0°	10°	20°	30°
C_Y	0.000	0.042	0.078	0.106

The value obtained is the following: $\frac{dC_Y}{d\delta_r} = 0.00356 \text{ deg}^{-1}$.

5.2 Yawing moment coefficient C_{M_z}

All rotations are considered positive if counterclockwise, and it is noted that the center of mass remains the same as the one used for the longitudinal analysis and the lateral force coefficient. To determine the direction of rotation, the rotation axis must be oriented toward the observer. It is important to note that the aircraft's axis Z_C is directed upward; therefore, a yaw that turns the nose to the left is considered positive. In Figure 5.5, the variation of the yawing moment coefficient with respect to the sideslip angle is shown for rudder deflections of 0° , 10° , 20° , and 30° .

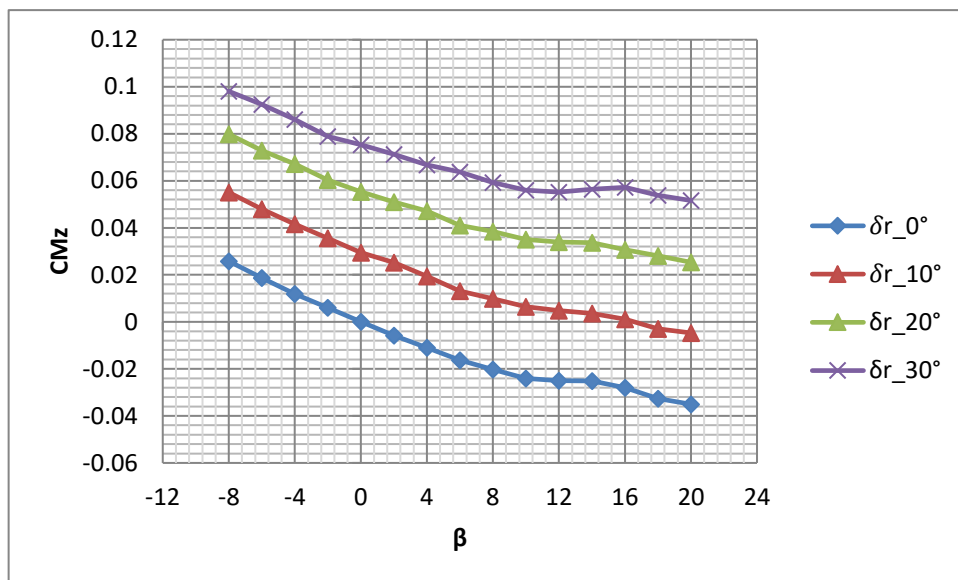


Figure 5.5 Variation of yaw moment coefficient C_{M_z} with sideslip angle β for different rudder deflections δr

Directional stability, also known as yaw stability, refers to an aircraft's ability to resist unwanted yawing motions and to realign itself with the relative wind following a disturbance. Physically, this corresponds to the generation of a yawing moment in response to a sideslip angle β , which tends to bring the aircraft's nose back toward the initial flight path. The directional stability derivative $dC_{M_z}/d\beta$, which represents the rate of change of the yawing moment coefficient with respect to the sideslip angle, results from the combined aerodynamic contributions of the fuselage, the wing, and the vertical tail. Each of these components plays a distinct role in the overall stability behavior.

- The fuselage typically contributes negatively to directional stability. When the aircraft is in a sideslip condition, the fuselage generates a lateral aerodynamic force that acts near the center of gravity, producing a yawing moment that tends to amplify the deviation rather than counteract it. This destabilizing effect is especially evident in aircraft with wide or bluff fuselage shapes. A particularly relevant example is the F-35 Lightning II, whose fuselage is designed with stealth and radar cross-section minimization in mind. Its wide, flattened shape enhances the destabilizing yawing moment in sideslip conditions. As a result, the directional instability introduced by the fuselage must be carefully counterbalanced by the stabilizing effects of the wing and vertical tail to ensure controllability and flight safety.
- The wing may contribute positively to directional stability, especially when it has a nonzero sweep angle. During a sideslip, the advancing wing (the one facing the relative wind) experiences an increased effective angle of attack and therefore generates more lift and induced drag than the retreating wing. This asymmetric aerodynamic loading results in a yawing moment that opposes the sideslip and supports stability. The magnitude of this effect depends on the wing planform and sweep angle.
- The vertical tail generally provides the most significant stabilizing contribution to directional stability. Located well aft of the center of gravity, it generates a lateral aerodynamic force during a sideslip that produces a strong restoring yawing moment.

The stability derivative was obtained using the SLOPE function in Excel in the β ranges where the aerodynamic coefficient exhibited a linear trend: $\frac{dC_{M_z}}{d\beta} = -0.0029 \text{ deg}^{-1}$.

The sign of the derivative indicates directional stability, considering that the reference frame with respect to which the moments are calculated is the Construction Reference Frame.

As the rudder deflection increases, the yawing moment coefficient also increases, since the vertical tail surface generates a progressively stronger lateral force. This force, acting behind the aircraft's center of gravity, produces an increasing moment about the yaw axis. The rise in the coefficient thus reflects the enhanced effectiveness of the rudder in producing directional moments, which is essential for the aircraft's control and maneuverability. As in the previous case, in order to evaluate the control derivative $dC_{M_z}/d\delta_r$, the sideslip angle is set to zero to isolate the effect of rudder deflection.

A linear interpolation is then performed between the values of the yawing moment coefficient corresponding to the previously defined rudder deflections. This approach allows for an accurate estimation of the yawing moment sensitivity with respect to the rudder input, while keeping the other aerodynamic conditions constant.

δ_r	0°	10°	20°	30°
C_{M_z}	0.000	0.029	0.055	0.075

The value obtained is the following: $\frac{dC_{M_z}}{d\delta_r} = 0.0025 \text{ deg}^{-1}$.

During rolling maneuvers, such as turns, an aircraft is subject to a phenomenon known as adverse yaw. This effect occurs when the aircraft's nose tends to yaw in the direction opposite to that of the intended turn. The primary cause lies in the differential aerodynamic drag generated by the wings: the descending wing, experiencing a lower relative airflow, produces less lift and drag, whereas the ascending wing, exposed to higher relative airflow, generates both increased lift and drag. This aerodynamic asymmetry induces a lateral force that results in an undesired yawing moment.

Adverse yaw is further amplified by dynamic effects related to the aircraft's rotation about the roll axis, which influence the pressure distribution over the wings. The result is a misalignment between the aircraft's longitudinal axis and its actual flight path, requiring corrective action.

5.3 Rolling moment coefficient C_{M_x}

Roll is the rotation of an aircraft about its longitudinal axis, typically caused by differential lift between the wings. In this analysis, the moments are calculated with respect to a fixed center of mass, which remains unchanged throughout the study. The adopted conventions for the rolling moment coefficient remain unchanged, therefore, since the x_c axis points toward the tailplane, a positive rolling rotation appears counterclockwise from the pilot's perspective. In practice, a positive flap deflection induces a positive rolling moment.

As with the directional analysis, in this case the flaps are used in a specific configuration: for the lateral analysis, flaperons, control surfaces that combine the functions of flaps and ailerons, are employed. In particular, they are deflected asymmetrically, enabling the generation of a rolling moment.

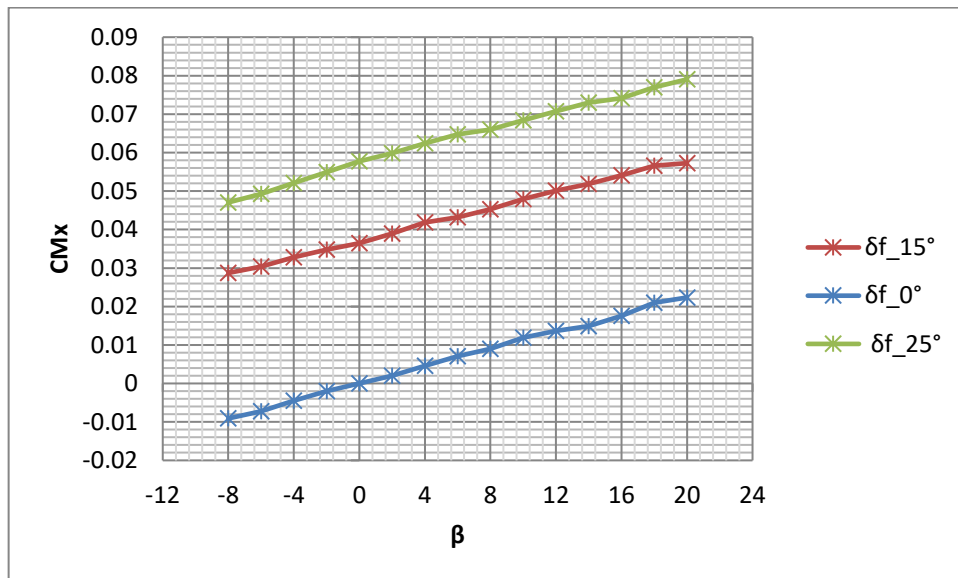


Figure 5.6 Rolling moment coefficient CM_x vs sideslip angle β for antisymmetric flap deflections δf

From Figure 5.6, multiple observations can be made regarding the aerodynamic behavior. Before addressing lateral control, this section discusses the dihedral effect, which represents the aircraft's roll stability in response to sideslip disturbances.

Consider an aircraft in steady, symmetric flight, with no rotations, no sideslip, and constant altitude. Now, suppose an external disturbance induces a wing inclination by an angle ϕ (roll). As a result, the total lift vector is no longer aligned vertically and fails to fully balance the aircraft's weight, leading to a loss of altitude. The downward vertical velocity component alters the flight path, so the relative wind no longer lies in the XZ symmetry plane. This introduces a nonzero sideslip angle β , i.e., an apparent lateral flow. If the roll causes the right wing to drop, the relative wind appears to come from the right. Due to the aircraft's directional stability, the fuselage tends to yaw into the flow, pointing the nose toward the right and slightly downward.

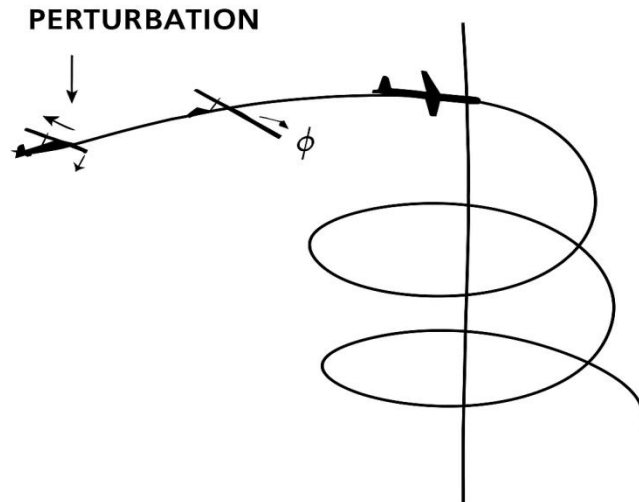


Figure 5.7 Spiral trajectory in absence of corrective moments

In the absence of a stabilizing rolling moment, the aircraft does not counteract the increasing lateral bank. This initiates a spiral mode, characterized by a progressive increase in roll and yaw, potentially leading to a steep descending spiral if no corrective action is taken. This phenomenon is illustrated in Figure 5.7.

The main contributor to lateral stability is the wing dihedral angle. In its absence, as in the case of the aircraft under analysis, the primary stabilizing effects come from the sweep of the wing and the sweep of the all-moving tailplane. The sweep provides a stabilizing effect in both the lateral and directional axes.

The stability derivative was obtained using the SLOPE function in Excel in the β ranges where the aerodynamic coefficient exhibited a linear trend: $\frac{dC_{M_x}}{d\beta} = 0.0012 \text{ deg}^{-1}$.

Figure 5.7 also shows that increasing the flap deflection results in an upward shift of the C_{M_x} curves, indicating a higher induced rolling moment. This trend is consistent with the expected control effect: asymmetric flap deflection modifies the spanwise lift distribution, producing a differential lift between the wings and thus an additional positive rolling moment. As a result, the control input directly biases the C_{M_x} values, while the slope of the curves, primarily associated with lateral stability due to sideslip, remains nearly unaffected.

A linear interpolation is then performed between the values of the rolling moment coefficient corresponding to flap deflections of $5^\circ, 10^\circ, 15^\circ$ and 20° . This approach allows for an accurate estimation of the rolling moment sensitivity with respect to the flap input, while keeping the other aerodynamic conditions constant.

δ_f	5°	10°	15°	20°
C_{M_x}	0.0131	0.0236	0.0366	0.0496

The value obtained is the following: $\frac{dC_{M_x}}{d\delta_f} = 0.00245 \text{ deg}^{-1}$.

When the rudder is deflected to generate a yawing moment, it produces a lateral aerodynamic force on the vertical tail. Since this force acts above the aircraft's center of mass, it not only induces yaw but also creates a rolling moment. This transverse interaction is known as the rudder cross-effect: a control input intended to yaw the nose of the aircraft also results in rotation about the longitudinal (roll) axis. The effect is especially noticeable in aircraft with high-mounted vertical stabilizers or large vertical surfaces. It is mathematically represented by the coupling derivative $dC_{M_x}/d\delta_r$ which quantifies the change in rolling moment due to the rudder deflection.

Figure 5.8 shows the variation of the rolling moment coefficient as a function of sideslip angle for rudder deflections of $0^\circ, 10^\circ, 20^\circ$, and 30° . According to the adopted conventions, positive rudder deflections generate a negative rolling moment.

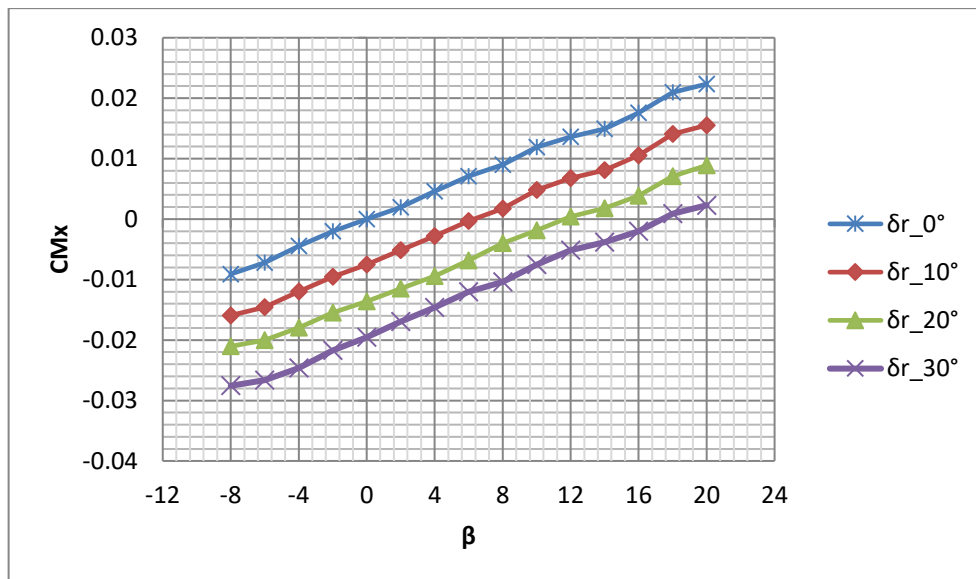


Figure 5.8 CM_x vs β for different rudder deflections δ_r

Similarly to the previous cases, the following control derivative was computed:

δ_r	0°	10°	20°	30°
C_{M_x}	0.0000	-0.0075	-0.0136	-0.0196

The value obtained is the following: $\frac{dC_{M_x}}{d\delta_r} = -0.00065 \text{ deg}^{-1}$.

A small derivative indicates that the rudder has a limited effect on the rolling moment, suggesting a compact vertical configuration, where the vertical tail forces do not generate large rolling moments because the vertical moment arm relative to the CG is short.

6. Conclusions

The study carried out allowed for a preliminary analysis of the aerodynamic characteristics of the F-35 Lightning II, highlighting its design features in terms of efficiency and maneuverability. The geometric modeling performed using OpenVSP proved effective for the simplified reconstruction of the aircraft's aerodynamic configuration, although with limitations due to the inability to represent complex structural details such as air intakes, control surfaces, and fairings.

The aerodynamic analysis conducted with VSPAERO yielded results qualitatively consistent with the expected behavior of a fifth-generation fighter. Although strongly dependent on the chosen position of the center of gravity, the evaluation of longitudinal and lateral-directional stability derivatives revealed a marginally stable behavior, with a clear tendency toward neutral stability. This reduced static margin is typical of modern combat aircraft designed to prioritize agility over inherent stability. Such reduced stability is effectively compensated by active control systems (fly-by-wire), ensuring controllability while maintaining high maneuverability. Due to approximations in the flow model used by VSPAERO, some inconsistencies were observed in the aerodynamic interaction between components, especially in the junction regions between wing, fuselage, and control surfaces. These effects, not fully captured by the VLM method, may affect aerodynamic coefficient distribution and overall performance assessment. Additionally, the integrated tool used to calculate parasite drag provided acceptable but approximate results, as it is based on semi-empirical correlations that do not fully reflect the aircraft's geometric and structural complexity.

More broadly, the F-35 Lightning II has marked a significant shift in military aviation, introducing a new operational paradigm based on stealth, sensor fusion, and multirole capabilities. Its global deployment has enhanced interoperability among allied forces and set new standards for modern aerial combat. Despite challenges related to cost and maintenance, the program continues to evolve through upgrades and will likely serve as a bridge to sixth-generation systems, playing a central role in the ongoing transformation of 21st-century air power.

Bibliography

- [1] Lockheed Martin. (2025). 5th Gen Capabilities - F-35 Lightning II. F-35.com. Retrieved June 2025, from <https://www.f35.com/f35/about/5th-gen-capabilities>.
- [2] Hill Air Force Base – 388th Fighter Wing. (2019, January 24). *Lethal F-35A heading to Red Flag 19-1*. U.S. Air Force.
- [3] Marien, T. (2021). Software Testing: VSPAERO [Master's thesis]. HAW Hamburg.
- [4] Pham, D., & Sheridan, C. (2021). Evaluation of VSPAERO Analysis Capabilities for Conceptual Design of Aircraft with Propeller-Blown Wings. NASA.
- [5] Bayon-Fernandez, T. (2022). CFD Tool VSPAERO: Actuator Disk and Flow Analysis. HAW Hamburg.
- [6] ICAS. (2022). Effects on the Wing's Aerodynamic Characteristics Due to Distributed Propulsion. ICAS Conference Proceedings.
- [7] Stevens, B. L., & Lewis, F. L. (2003). *Aircraft Control and Simulation* (2nd ed.). Wiley-Interscience.
- [8] Nelson, R. C. (1998). *Flight Stability and Automatic Control* (2nd ed.). McGraw-Hill.
- [9] Etkin, B., & Reid, L. D. (1996). *Dynamics of Flight: Stability and Control* (3rd ed.). Wiley.